

EPFL

SEMESTER PROJECT

Minimal Rational Interpolation for Time-Harmonic Maxwell's Equations

Fabio Matti

supervised by
Prof. Fabio Nobile
Dr. Davide Pradovera

May 25, 2022

ABSTRACT

Minimal Rational Interpolation (MRI) provides an efficient and reliable way to approximate the dependence of a characteristic quantity of a model on one of its parameters. The focus of this report is put on the Greedy Minimal Rational Interpolation (gMRI) algorithm and particularly on way to enhance its performance. This algorithm is then applied to three example problems concerning the time-harmonic Maxwell's equations in the frequency domain. A brief evaluation of the advantages and disadvantages of gMRI as compared to conventional approaches for finding quantities, such as resonant modes, of interest for problems of this type is conducted.

CONTENTS

1	Introduction	4
2	Finite element discretization of the time-harmonic Maxwell's equations	5
2.1	Vector potential formulation of the time-harmonic Maxwell's equations	5
2.2	Weak formulation for the time-harmonic potential equation	6
2.3	Examples	6
2.3.1	Two-dimensional resonant cavity	7
2.3.2	Imperfect conductor	8
2.3.3	Waveguide	8
3	Finite element approximation with FEniCS	9
3.1	Theory (come up with better title)	9
3.2	Demonstration (come up with better title)	9
4	Minimal rational interpolation for the time-harmonic Maxwell's equations	11
4.1	Motivation	11
4.2	Minimal rational interpolation	11
4.3	Greedy minimal rational interpolation	11
4.4	Properties of rational interpolants in barycentric coordinates	12
4.5	Finding roots of rational functions	12
4.6	Optimization tricks for greedy minimal rational interpolation	13
4.6.1	Additive Householder decomposition	13
4.6.2	Stability of singular value decomposition	13
4.6.3	(Think of a title)	15
5	Examples	16
5.1	Two-dimensional rectangular cavity	16
5.2	Imperfectly conducting boundaries	18
5.3	Dual mode circular waveguide filter	19
6	Conclusion and outlook	21
7	Appendix	23
7.1	Detailed derivation for the weak formulation of the time-harmonic potential equation	23

1 INTRODUCTION

A wide class of problems in physics and engineering concerns itself with the study of the dependence of a model on one of its parameters. Of interest is usually a characteristic quantity that covaries with said parameter. Unless the system allows for an analytical solution, one may usually only find numerical solutions to the system for discrete values of the parameter. Minimal Rational Interpolation (MRI) offers a way to locally approximate the continuous dependence of a model on one of its parameters. The approach has proven effective and efficient (both memory- and computation wise) in applications on Helmholtz-type problems [3, 1].

Central to this report are time-harmonic electromagnetic problems, whose parameter is the (angular) frequency. These problems are governed by the time-harmonic Maxwell's equations. Choosing the quantity of interest to be a vector potential, these equations reduce to a single curl-curl equation. A justification for why a rational interpolation approach is appropriate for this class of problems will be presented in Section 4.1.

The first few pages in this report are a short guide for finding numerical solutions to the time-harmonic Maxwell's equations using the Finite Element Method (FEM). These solutions are then used in the core of this report, which gives a description of the Greedy Minimal Rational Interpolation (gMRI) algorithm. Properties of and optimization tricks for the gMRI are shown. In the end, three applications of the method are studied and discussed: the resonant modes of a two-dimensional resonant cavity, the two-dimensional cavity with an imperfectly conducting boundary, and lastly the scattering coefficients of a Dual-Mode Circular Waveguide Filter (DMCWF).

2 FINITE ELEMENT DISCRETIZATION OF THE TIME-HARMONIC MAXWELL'S EQUATIONS

Minimal Rational Interpolation (MRI) requires the knowledge of the solution of the problem for multiple values of the model parameter that is of interested. A way of obtaining these solutions is the Finite Element Method (FEM). For that purpose, I now derive a strong formulation for the time-harmonic Maxwell problem and subsequently convert it to its corresponding weak formulation.

2.1 VECTOR POTENTIAL FORMULATION OF THE TIME-HARMONIC MAXWELL'S EQUATIONS

I assume that all quantities in this section are smooth enough to perform the necessary vector calculus manipulations.

Let \mathbf{E} denote an electric field, \mathbf{B} a magnetic field strength, ρ an electric charge density, and \mathbf{j} an electric current density. Maxwell's equations are stated in [8] as

$$\nabla \cdot (\epsilon \mathbf{E}) = \rho \quad (2.1)$$

$$\nabla \cdot \mathbf{B} = 0 \quad (2.2)$$

$$\nabla \times \mathbf{E} = -\partial_t \mathbf{B} \quad (2.3)$$

$$\nabla \times (\mu^{-1} \mathbf{B}) = \partial_t (\epsilon \mathbf{E}) + \mathbf{j} \quad (2.4)$$

with ϵ being the permittivity and μ the permeability (whose names let alone their values I always tend to forget).

Equation (2.2) motivates the expression of the magnetic field $\mathbf{B} = \nabla \times \mathbf{u}$ in terms of a vector valued function \mathbf{u} , the vector potential (in literature commonly denoted with \mathbf{A}). Similarly, (2.3) suggests rewriting the electric field $\mathbf{E} = -\nabla \phi - \partial_t \mathbf{u}$ using a scalar function ϕ , referred to as the scalar potential.

The physical quantities \mathbf{E} and \mathbf{B} remain unchanged if we transform $\mathbf{u} \rightarrow \mathbf{u}' = \mathbf{u} + \nabla \psi$ or $\phi \rightarrow \phi' = \phi - \partial_t \psi$ for arbitrary functions ψ . A convenient choice of ψ is suggested in [6] to be

$$\psi = \int_0^t \phi dt' \quad (2.5)$$

which transforms $\phi \rightarrow \phi' = 0$ and $\mathbf{u} \rightarrow \mathbf{u}' = \mathbf{u} + \nabla \int_0^t \phi dt'$. Thus, the expressions for the electrical and magnetic field become

$$\mathbf{E} = -\partial_t \mathbf{u} \quad (2.6)$$

$$\mathbf{B} = \nabla \times \mathbf{u} \quad (2.7)$$

where I have subtly renamed the variable \mathbf{u}' to \mathbf{u} for simplicity.

Plugging the identities (2.6) and (2.7) into (2.4) yields

$$\nabla \times (\mu^{-1} \nabla \times \mathbf{u}) = -\epsilon \partial_t^2 \mathbf{u} + \mathbf{j} \quad (2.8)$$

For the rest of this report, I restrict myself to vector potentials \mathbf{u} that exhibit a harmonic dependence on time t , i.e. may be factorized into a term solely depending

on the position \mathbf{x} and a complex exponential depending on time

$$\mathbf{u}(\mathbf{x}, t) = \mathbf{u}(\mathbf{x}) \exp(i\omega t) \quad (2.9)$$

Substituting this expression into (2.8) and rearranging a little results in the

Time-harmonic potential equation

$$\nabla \times (\mu^{-1} \nabla \times \mathbf{u}) - \epsilon \omega^2 \mathbf{u} = \mathbf{j} \quad (2.10)$$

2.2 WEAK FORMULATION FOR THE TIME-HARMONIC POTENTIAL EQUATION

Equation (2.10) may be multiplied by a vector-valued function $\mathbf{v} \in H_{\text{curl}}(\Omega)$, where

$$H_{\text{curl}}(\Omega) = \{\mathbf{u} : \Omega \rightarrow \mathbb{C}, \text{ such that } \mathbf{u} \in L_2(\mathbb{C})^3, \nabla \times \mathbf{u} \in L_2(\mathbb{C})^3\} \quad (2.11)$$

and then integrated over the whole computational domain Ω to obtain

$$\int_{\Omega} (\nabla \times (\mu^{-1} \nabla \times \mathbf{u})) \cdot \mathbf{v} - \omega^2 \int_{\Omega} \epsilon \mathbf{u} \cdot \mathbf{v} = \int_{\Omega} \mathbf{j} \cdot \mathbf{v} \quad (2.12)$$

This may further be simplified (2.12) to (I allow myself to spare you the details of this computation, but put a proper derivation in an appendix at the end of the report):

Weak formulation of the time-harmonic potential equation

$$\int_{\Omega} (\mu^{-1} \nabla \times \mathbf{u}) \cdot (\nabla \times \mathbf{v}) - \omega^2 \int_{\Omega} \epsilon \mathbf{u} \cdot \mathbf{v} = \int_{\Omega} \mathbf{j} \cdot \mathbf{v} + \int_{\partial\Omega} \underbrace{((\mu^{-1} \nabla \times \mathbf{u}) \times \mathbf{n}) \cdot \mathbf{v}}_{=\mathbf{g}} \quad (2.13)$$

where \mathbf{n} denotes the surface normal to the boundary $\partial\Omega$ of the computational domain Ω .

Boundary conditions on the electric field \mathbf{E} may be most easily enforced in a Dirichlet-type fashion through the relation (2.6) and the assumption (2.9)

$$\mathbf{u}|_{\Gamma_D} = -\frac{1}{i\omega} \mathbf{E}|_{\Gamma_D} \quad (2.14)$$

Those on the magnetic field \mathbf{B} through a Neumann-type condition following from (2.7) and again (2.9)

$$\mathbf{g}|_{\Gamma_N} = (\mu^{-1} \mathbf{B}|_{\Gamma_N}) \times \mathbf{n} \quad (2.15)$$

2.3 EXAMPLES

I will now specialize and simplify this weak formulation for three different applications which will be studied in Section 5. To show you that these problems are intimately related problems, I refer you to Figure 2.1.

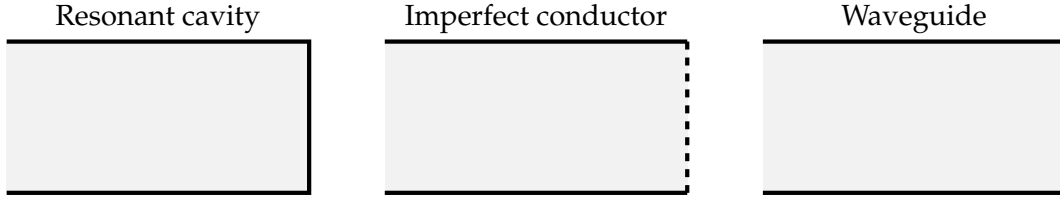


FIGURE 2.1 – Schematic visualization of the most trivial case for each of the boundary configurations that will be analyzed in Section 5. The perfectly conducting boundaries are drawn in black, while the imperfectly conducting boundary appears dashed. Inlets and exits are left unmarked.

2.3.1 TWO-DIMENSIONAL RESONANT CAVITY

I refer to a resonant cavity as a region Ω enclosed by a boundary $\partial\Omega$. The boundary can be subdivided into one (or more) inlets Γ_N and a perfect conducting wall $\Gamma_D = \partial\Omega \setminus \Gamma_N$ (see Figure 2.2 for an abstract visualization of such a cavity).

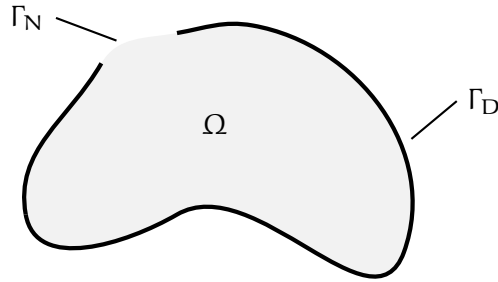


FIGURE 2.2 – An abstract example of a two-dimensional resonant cavity enclosing a domain Ω with a perfectly conducting boundary Γ_D and featuring a single inlet Γ_N .

Suppose the current density $\mathbf{j} \equiv 0$ and orient the coordinate system in such a way that $\mathbf{u} = u_z \mathbf{e}_z$ and $\mathbf{v} = v_z \mathbf{e}_z$. Consequently, the scalar product of the two curls in Equation (??) simplifies to the scalar product of two gradients:

$$(\mu^{-1} \nabla \times \mathbf{u}) \cdot (\nabla \times \mathbf{v}) = (\mu^{-1} \nabla u_z) \cdot (\nabla v_z) \quad (2.16)$$

Denote by g_z the component of \mathbf{g} in the z -direction along the inlet Γ_N . These simplifications allow the conversion of (2.13) into the weak formulation for a two-dimensional resonant cavity

$$\int_{\Omega} (\mu^{-1} \nabla u_z) \cdot (\nabla v_z) - \omega^2 \int_{\Omega} \epsilon u_z v_z = \int_{\partial\Omega} g_z v_z \quad (2.17)$$

Now, let \mathbf{E} and \mathbf{B} refer to the electric and magnetic fields inside the cavity. For now, I distinguish between two types of boundaries:

For the perfectly conducting boundary Γ_D , treated in [8], it holds that

$$\mathbf{n} \times \mathbf{E} = 0, \text{ on } \Gamma_D \quad (2.18)$$

For the boundaries in a two-dimensional resonant cavity (see Figure 2.2), this only holds true if $E_z = 0$, which translates to the Dirichlet boundary condition $\mathbf{u}|_{\Gamma_D} = 0$ in light of (2.14).

For the inlet, it is easiest to enforce the boundary condition through the magnetic field \mathbf{B} in exactly the way proposed in (2.15) (assuming $\mathbf{n} = -\mathbf{e}_x$ as will always be the case in Section 5, cf. Figure 5.1):

$$g_z = ((\mu^{-1}\mathbf{B}) \times (-\mathbf{e}_x))_z = \mu^{-1}B_x, \text{ on } \Gamma_N \quad (2.19)$$

2.3.2 IMPERFECT CONDUCTOR

To simulate an imperfect boundary Γ_I , also called impedance boundary in literature, [8] suggests to replace the integrand \mathbf{g} that appeared in (2.13) with

$$\mathbf{g} = (\mu^{-1}\nabla \times \mathbf{u}) \times \mathbf{n} = i\omega\lambda(\mathbf{n} \times \mathbf{u}) \times \mathbf{n} \text{ on } \Gamma_D \quad (2.20)$$

with a parameter $\lambda > 0$ I will henceforth refer to as the impedance. Supposing that $\mathbf{u} = u_z\mathbf{e}_z$ and only treating a two-dimensional domain, this condition simplifies to (using the fact that $\mathbf{n} \perp \mathbf{u}$ and $\|\mathbf{n}\| = 1$, so $(\mathbf{n} \times \mathbf{u}) \times \mathbf{n} = \mathbf{u}$, as is demonstrated in the appendix at the end of this report)

$$g_z = i\omega\lambda u_z \text{ on } \Gamma_D \quad (2.21)$$

Therefore, an impedance boundary can be treated in almost the same way as a Neumann boundary in the two-dimensional weak formulation (2.17) of a resonant cavity.

2.3.3 WAVEGUIDE

Going back to (2.13) and this time staying in three dimensions, we again assume no electric current density $\mathbf{j} \equiv 0$ is present. I suppose that the inlet is located at a constant x -value, such that the surface normal to this inlet is $-\mathbf{e}_x$. Conveniently, the example in Section 5.3 happens to be set up in just this way. For an incoming magnetic field at the inlet Γ_i with $\mathbf{B}|_{\Gamma_i} = B_0\mathbf{e}_y$, we see from (2.15) that this may be modelled by setting $\mathbf{g}|_{\Gamma_i} = -\mu^{-1}B_0\mathbf{e}_z$. At the “exit” Γ_e , we set $\mathbf{g}|_{\Gamma_e} = \mathbf{0}$.

3 FINITE ELEMENT APPROXIMATION WITH FENICS

3.1 THEORY (COME UP WITH BETTER TITLE)

Along the lines of [4].

See immediately that the weak formulation (2.13) assumes the shape

$$\text{Find } \mathbf{u} \in V, \text{ such that } a_\omega(\mathbf{u}, \mathbf{v}) = L(\mathbf{v}), \forall \mathbf{v} \in V_0 \quad (3.1)$$

with the bilinear form

$$a_\omega(\mathbf{u}, \mathbf{v}) = \int_{\Omega} (\mu^{-1} \nabla \times \mathbf{u}) \cdot (\nabla \times \mathbf{v}) - \omega^2 \int_{\Omega} \epsilon \mathbf{u} \cdot \mathbf{v} \quad (3.2)$$

and the linear form

$$L(\mathbf{u}) = \int_{\Omega} \mathbf{j} \cdot \mathbf{v} + \int_{\partial\Omega} \mathbf{g} \cdot \mathbf{v} \quad (3.3)$$

3.2 DEMONSTRATION (COME UP WITH BETTER TITLE)

In the style of [4]. Problem (2.13) with Ω being a cubic cavity with an inlet on one side and all other sides with $\mu = \epsilon = 0, \mathbf{j} = 0$ for simplicity.

Required packages

```
0 | import numpy as np
1 | import fenics as fen
2 | import matplotlib.pyplot as plt
```

Mesh

```
5 | nx, ny, nz = 10, 10, 10
6 | mesh = fen.UnitCubeMesh(nx, ny, nz)
```

Function space (Nédélec elements of the first kind [8])

```
9 | V = fen.FunctionSpace(mesh, 'N1curl', 1)
```

Inlet (at $x = 0$)

```
12 | class Inlet(fen.SubDomain):
13 |     def inside(self, x, on_boundary):
14 |         return on_boundary and fen.near(x[0], 0)
```

PEC boundary

```
17 | class PECWalls(fen.SubDomain):
18 |     def inside(self, x, on_boundary):
19 |         return on_boundary and not Inlet().inside(x, on_boundary)
```

Boundary ids

```
22 | boundary_id = fen.MeshFunction('size_t', mesh, mesh.topology().dim()-1)
23 | boundary_id.set_all(0)
24 | Inlet().mark(boundary_id, 1)
25 | PECWalls().mark(boundary_id, 2)
```

Dirichlet boundary (0 for PEC, because Nédélec)

```
28 | u_D = fen.Expression(('0.0', '0.0', '0.0'), degree=2)
29 | bc = fen.DirichletBC(V, u_D, boundary_id, 2)
```

Neumann boundary (1 for ...)

```
32 g_N = fen.Expression(('0.0', '0.0', '1.0'), degree=2)
33 ds = fen.Measure('ds', subdomain_data=boundary_id)
```

Trial and test functions

```
36 u = fen.TrialFunction(V)
37 v = fen.TestFunction(V)
```

Neumann boundary integral term

```
40 N = fen.assemble(fen.dot(g_N, v) * ds(2))
```

Stiffness matrix

```
43 K = fen.assemble(fen.dot(fen.curl(u), fen.curl(v)) * fen.dx)
44 bc.apply(K)
```

Mass matrix

```
47 M = fen.assemble(fen.dot(u, v) * fen.dx)
48 bc.zero(M)
```

L2 norms

```
51 def L2_norm(u):
52     u_vec = u.vector().get_local()
53     return pow(((M * u_vec) * u_vec).sum(), 0.5)
```

Solution at frequencies

```
56 omegas = np.linspace(6.2, 6.8, 200)
57 norms = []
58 u = fen.Function(V)
59 for omega in omegas:
60     fen.solve(K - omega**2 * M, u.vector(), N)
61     norms.append(L2_norm(u))
```

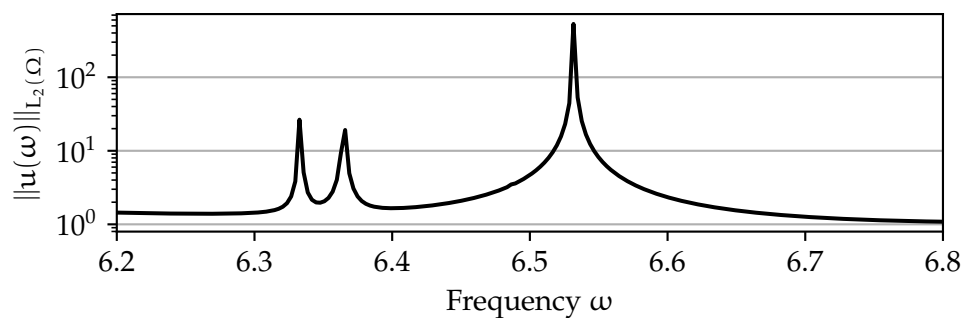


FIGURE 3.1 – TODO.

4 MINIMAL RATIONAL INTERPOLATION FOR THE TIME-HARMONIC MAXWELL'S EQUATIONS

Let $\mathbf{u} : \mathbb{C} \rightarrow \mathbb{C}^3$. Given $\mathbf{u}_j = \mathbf{u}(\omega_j)$ for $j \in \{1, \dots, S\}$. Want to find a surrogate

$$\tilde{\mathbf{u}}(\omega) \approx \mathbf{u}(\omega) \quad (4.1)$$

4.1 MOTIVATION

Equations of the type (2.10), in the most simple case (dropping all constants)

$$\nabla \times (\nabla \times \mathbf{u}) - \omega^2 \mathbf{u} = \mathbf{j} \quad (4.2)$$

Writing the double-curl operator in terms of a matrix $\underline{\mathbf{A}}$

$$\mathbf{u} = (\underline{\mathbf{A}} - \omega^2 \mathbf{1})^{-1} \mathbf{j} \quad (4.3)$$

Eigenvalue decomposition $\underline{\mathbf{A}} = \underline{\mathbf{V}} \underline{\mathbf{\Lambda}} \underline{\mathbf{V}}^H$ leads us to a form proposed in [2]

$$\mathbf{u} = \underline{\mathbf{V}} (\underline{\mathbf{\Lambda}} - \omega^2 \mathbf{1})^{-1} \underline{\mathbf{V}}^H \mathbf{j} = \sum_i \frac{\mathbf{v}_i \mathbf{v}_i^H \mathbf{j}}{\lambda_i - \omega^2} \quad (4.4)$$

which follows from the fact that $\underline{\mathbf{\Lambda}}$ is diagonal, hence also $(\underline{\mathbf{\Lambda}} - \omega^2 \mathbf{1})^{-1}$. Here, we denoted the diagonal elements of $\underline{\mathbf{\Lambda}}$ with λ_i (the eigenvalues of $\underline{\mathbf{A}}$) and the columns of $\underline{\mathbf{V}}$ with \mathbf{v}_i (the eigenvectors of $\underline{\mathbf{A}}$).

Hence, it would make sense to search for an approximation of the solution \mathbf{u} that is able to “model” the singularities at $\omega^2 = \lambda_i$, e.g. rational polynomials

$$\tilde{\mathbf{u}}(\omega) = \frac{P(\omega)}{Q(\omega)} \quad (4.5)$$

4.2 MINIMAL RATIONAL INTERPOLATION

[3]

Algorithm 1 Minimal rational interpolation

Require: $\omega_1, \dots, \omega_S$

Require: $\mathbf{U} = [\mathbf{u}(\omega_1), \dots, \mathbf{u}(\omega_S)]$

Compute \mathbf{G} with $g_{ij} = \langle \mathbf{u}(\omega_i), \mathbf{u}(\omega_j) \rangle_M$, $i, j \in \{1, \dots, S\}$

Compute the singular value decomposition $\mathbf{G} = \mathbf{V} \mathbf{\Sigma} \mathbf{V}^H$

Define $\mathbf{q} = \mathbf{V}[:, S]$

Define $\tilde{\mathbf{u}}(\omega) = P(\omega)/Q(\omega)$ with $P(\omega) = \sum_{j=1}^S \frac{q_j \mathbf{u}(\omega_j)}{\omega - \omega_j}$ and $Q(\omega) = \sum_{j=1}^S \frac{q_j}{\omega - \omega_j}$

▷ Snapshot matrix

▷ Gramian matrix

4.3 GREEDY MINIMAL RATIONAL INTERPOLATION

Greedy Minimal Rational Interpolation (gMRI)

[1]

Algorithm 2 Greedy minimal rational interpolation

Require: $\tau > 0$ ▷ Relative L_2 -error tolerance
Require: $\Omega_{\text{test}} = \{\omega_i\}_{i=1}^M$ ▷ Set of candidate support points
Require: $a_\omega(u, v) = L(v)$ ▷ Finite element formulation of the problem
 Choose $\omega_1, \dots, \omega_t \in \Omega_{\text{test}}$ ▷ Usually the smallest and largest element
 Remove $\omega_1, \dots, \omega_t$ from Ω_{test}
 Solve $a_{\omega_i}(u_i, v) = L(v)$ for $i \in \{1, \dots, t\}$
 Build surrogate $\tilde{u}_t = P_t(\omega)/Q_t(\omega)$ using the solutions u_1, \dots, u_t
while $\Omega_{\text{test}} \neq \emptyset$ **do**
 $\omega_{t+1} \leftarrow \operatorname{argmin}_{\omega \in \Omega_{\text{test}}} |Q_t(\omega)|$
 Solve $a_{\omega_{t+1}}(u_{t+1}, v) = L(v)$
 Build surrogate $\tilde{u}_{t+1} = P_{t+1}(\omega)/Q_{t+1}(\omega)$ using the solutions u_1, \dots, u_{t+1}
 if $\|u_{t+1}(\omega_{t+1}) - \tilde{u}_{t+1}(\omega_{t+1})\|_M / \|u_{t+1}(\omega_{t+1})\|_M < \tau$ **then return**
 end if
 $t \leftarrow t + 1$
end while

4.4 PROPERTIES OF RATIONAL INTERPOLANTS IN BARYCENTRIC COORDINATES

The rational surrogate \tilde{u} can be rewritten as

$$\begin{aligned}
 \tilde{u}(\omega) &= \sum_{j=1}^S \frac{q_j \mathbf{u}(\omega_j)}{\omega - \omega_j} / \sum_{j=1}^S \frac{q_j}{\omega - \omega_j} \\
 &= \sum_{j=1}^S \prod_{\substack{i=0 \\ i \neq j}}^S (\omega - \omega_i) q_j \mathbf{u}(\omega_j) / \sum_{j=1}^S \prod_{\substack{i=0 \\ i \neq j}}^S (\omega - \omega_i) q_j
 \end{aligned} \tag{4.6}$$

Therefore, if the rational surrogate \tilde{u} is evaluated at one of the interpolation nodes ω_i , $\mathbf{u}(\omega_i)$ is recovered.

If the rational surrogate \tilde{u} is evaluated in a zero $\bar{\omega}$ of the denominator $Q(\bar{\omega}) = 0$, we observe a pole, unless $P(\bar{\omega})$ happens to vanish too.

4.5 FINDING ROOTS OF RATIONAL FUNCTIONS

Then used for determining resonant modes (i.e. where $Q(\omega) = 0$) [7]

Defining

$$v_i = (\omega - \omega_i)^{-1} \tag{4.7}$$

and requiring

$$0 = Q(\omega) = \sum_{i=1}^S q_i v_i(\omega) \tag{4.8}$$

can be equivalently expressed as a generalized eigenvalue problem

$$\underline{\mathbf{A}} \mathbf{u} = \omega \underline{\mathbf{B}} \mathbf{u} \tag{4.9}$$

with

$$\underline{\mathbf{A}} = \begin{pmatrix} 0 & q_1 & q_2 & \dots & q_S \\ 1 & \omega_1 & & & \\ 1 & & \omega_2 & & \\ \vdots & & & \ddots & \\ 1 & & & & \omega_S \end{pmatrix} \text{ and } \underline{\mathbf{B}} = \begin{pmatrix} 0 & & & & \\ & 1 & & & \\ & & 1 & & \\ \vdots & & & \ddots & \\ & & & & 1 \end{pmatrix} \quad (4.10)$$

4.6 OPTIMIZATION TRICKS FOR GREEDY MINIMAL RATIONAL INTERPOLATION

4.6.1 ADDITIVE HOUSEHOLDER DECOMPOSITION

Algorithm 1 requires the computation of the Singular Value Decomposition (SVD) of the Gramian matrix $\underline{\mathbf{G}}$. An alternative is to compute the QR decomposition of the snapshot matrix $\underline{\mathbf{U}} = [\mathbf{u}(\omega_1), \dots, \mathbf{u}(\omega_S)]$. Since

$$\underline{\mathbf{G}} = \underline{\mathbf{U}}^H \underline{\mathbf{M}} \underline{\mathbf{U}} \quad (4.11)$$

with the matrix $\underline{\mathbf{M}}$ representing the finite element L_2 inner product Ω . A QR decomposition with respect to the inner product $\langle \mathbf{u}, \mathbf{v} \rangle = \mathbf{u}^H \underline{\mathbf{M}} \mathbf{v}$ yields $\underline{\mathbf{U}} = \underline{\mathbf{Q}} \underline{\mathbf{R}}$ with $\underline{\mathbf{Q}}^H \underline{\mathbf{M}} \underline{\mathbf{Q}} = \underline{\mathbf{I}}$. When plugging this into (4.11) one sees

$$\underline{\mathbf{G}} = (\underline{\mathbf{Q}} \underline{\mathbf{R}})^H \underline{\mathbf{M}} (\underline{\mathbf{Q}} \underline{\mathbf{R}}) = \underline{\mathbf{R}}^H \underline{\mathbf{R}} \quad (4.12)$$

Let the SVD of $\underline{\mathbf{R}}$ be

$$\underline{\mathbf{R}} = \underline{\mathbf{W}} \underline{\mathbf{S}} \underline{\mathbf{V}}^H \quad (4.13)$$

Inserting this into (4.12) results in

$$\underline{\mathbf{G}} = (\underline{\mathbf{W}} \underline{\mathbf{S}} \underline{\mathbf{V}}^H)^H \underline{\mathbf{W}} \underline{\mathbf{S}} \underline{\mathbf{V}}^H = \underline{\mathbf{V}} \underline{\mathbf{S}}^2 \underline{\mathbf{V}}^H \quad (4.14)$$

which yields the SVD of the Gramian matrix $\underline{\mathbf{G}}$.

There is one big benefit to taking the route via the SVD for gMRI: When extending the snapshot matrix by an additional snapshot $\mathbf{u}(\omega_{S+1})$, the resulting triangular matrix $\underline{\mathbf{R}}^{(S+1)}$ from a QR decomposition on this extended snapshot matrix only differs from the (possibly) already computed $\underline{\mathbf{R}}^{(S)}$ only in the last column. Thus, it is possible to fully reuse results obtained in previous iterations in gMRI and therefore significantly increase computational efficiency.

I developed such an additive QR decomposition in Algorithm 3, which results from an adaption of the Householder triangularization algorithm found in [10].

4.6.2 STABILITY OF SINGULAR VALUE DECOMPOSITION

Can check stability with singular values $\sigma_1, \dots, \sigma_S$ in $\underline{\mathbf{S}}$. Need smallest singular values to differ from each other. This conditioning can be estimated with the relative spectral range [9]

$$\frac{\sigma_{S-1} - \sigma_S}{\sigma_1 - \sigma_S} \quad (4.15)$$

Algorithm 3 Additive Householder triangularization

Require: $U[1 \dots s, 1 \dots N]$ \triangleright Next snapshot matrix
Require: $R[1 \dots S, 1 \dots S]$ \triangleright Previous triangular matrix
Require: $E[1 \dots S, 1 \dots N]$ \triangleright Previous orthonormal matrix
Require: $V[1 \dots S, 1 \dots N]$ \triangleright Previous Householder matrix

Extend size of R to $(S + s) \times (S + s)$
Extend E with S orthonormal columns to $(S + s) \times N$
Extend size of V to $(S + s) \times N$
for $j = S + 1 : S + s$ **do**
 $u = U[j]$
 for $k = 1 : j - 1$ **do**
 $u \leftarrow u - 2 \langle V[k, :], u \rangle_M V[k, :]$
 $R[k, j] \leftarrow \langle E[k, :], u \rangle_M$
 $u \leftarrow u - R[k, j] E[k, :]$
 end for
 $R[j, j] \leftarrow \|u\|_M$
 $\alpha \leftarrow \langle E[j, :], u \rangle_M$
 if $|\alpha| \neq 0$ **then**
 $E[j, :] \leftarrow E[j, :] (-\alpha / |\alpha|)$
 end if
 $V[j, :] \leftarrow R[j, j] E[j, :] - u$
 $V[j, :] \leftarrow V[j, :] - \langle E[S + 1 : j], V[j, :] \rangle_M E[S + 1 : j, :]$
 $\sigma \leftarrow \|V[j, :]\|_M$
 if $\sigma \neq 0$ **then**
 $V[j, :] \leftarrow V[j, :] / \sigma$
 else
 $V[j, :] \leftarrow E[j, :]$
 end if
end for

4.6.3 (THINK OF A TITLE)

Denote $\underline{\mathbf{U}} = [\mathbf{u}(\omega_1), \dots, \mathbf{u}(\omega_S)]$ snapshot matrix. Let

$$\mathring{\mathbf{u}}(\omega) = \sum_{j=1}^S \frac{q_j \mathbf{e}_j}{\omega - \omega_j} / \sum_{j=1}^S \frac{q_j}{\omega - \omega_j} \quad (4.16)$$

with the canonical basis vectors $\{\mathbf{e}_j\}_j$, and denote $\mathring{\underline{\mathbf{U}}} = [\mathring{\mathbf{u}}(\omega_1), \dots, \mathring{\mathbf{u}}(\omega_S)]$. Inspecting the rational surrogate (defined in Algorithm 1) closely, it is apparent that

$$\tilde{\mathbf{u}}(\omega) = \underline{\mathbf{U}} \mathring{\mathbf{u}}(\omega) \quad (4.17)$$

Therefore, a rational surrogate is fully characterized by just S numbers $\{q_1, \dots, q_S\}$ and the locations of the interpolation nodes $\{\omega_1, \dots, \omega_S\}$.

Additionally, let

$$\hat{\mathbf{u}}(\omega) = \underline{\mathbf{R}} \mathring{\mathbf{u}}(\omega) \quad (4.18)$$

with $\underline{\mathbf{R}}$ being the triangular matrix stemming from the QR decomposition $\underline{\mathbf{U}} = \underline{\mathbf{Q}} \underline{\mathbf{R}}$. The original rational surrogate can again be recovered via

$$\tilde{\mathbf{u}}(\omega) = \underline{\mathbf{Q}} \hat{\mathbf{u}}(\omega) \quad (4.19)$$

$\hat{\mathbf{u}}(\omega)$ greatly simplifies the computation of the relative error in gMRI (Algorithm 2)

$$\|\mathbf{u}_{t+1}(\omega_{t+1}) - \tilde{\mathbf{u}}_{t+1}(\omega_{t+1})\|_M = \|\underline{\mathbf{Q}} \mathbf{r}_{t+1} - \underline{\mathbf{Q}} \hat{\mathbf{u}}_{t+1}(\omega_{t+1})\|_M = \|\mathbf{r}_{t+1} - \hat{\mathbf{u}}_{t+1}(\omega_{t+1})\|_M \quad (4.20)$$

and also

$$\|\mathbf{u}\|_M^2 \approx \|\hat{\mathbf{u}}\|_M^2 = \|\underline{\mathbf{U}} \mathring{\mathbf{u}}(\omega)\|_M^2 = \mathring{\mathbf{u}}(\omega)^H \underbrace{\underline{\mathbf{U}}^H \underline{\mathbf{M}} \underline{\mathbf{U}}}_{=\underline{\mathbf{G}}=\underline{\mathbf{R}}^H \underline{\mathbf{R}}} \mathring{\mathbf{u}}(\omega) = \hat{\mathbf{u}}(\omega)^H \hat{\mathbf{u}}(\omega) = \|\hat{\mathbf{u}}(\omega)\|^2 \quad (4.21)$$

Thus, the norm computation can be reduced to the much simpler euclidean norm.

5 EXAMPLES

5.1 TWO-DIMENSIONAL RECTANGULAR CAVITY

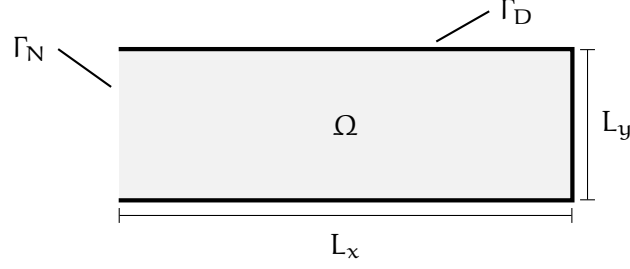
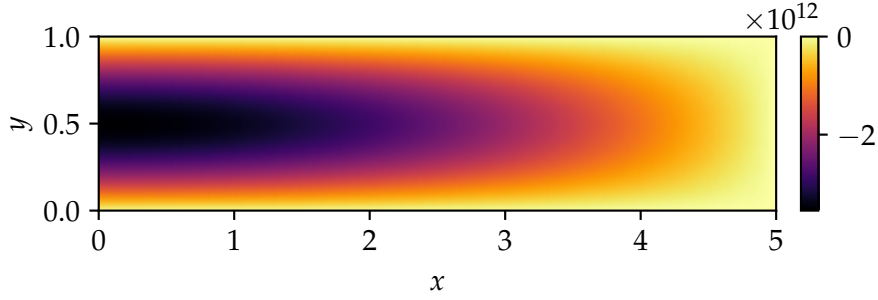
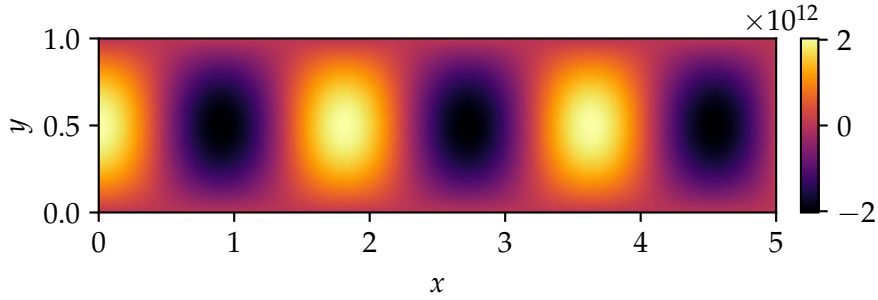


FIGURE 5.1 – TODO.



(A) First resonant frequency $\omega = 3.159$.



(B) Fifth resonant frequency $\omega = 4.675$.

FIGURE 5.2 – Caption.

For $\|\mathbf{u}\|_{L_2(\Omega)}^2 = \int_{\Omega} \|\mathbf{u}\|^2$
 Analytical eigenfrequencies

$$\omega_{n,m} = \pi \sqrt{\left(\frac{2n+1}{2L_x}\right)^2 + \left(\frac{m}{L_y}\right)^2}, \quad n \in \{0, 1, \dots\}, \quad m \in \{1, 2, \dots\} \quad (5.1)$$

Numerical eigenfrequencies, solve generalized (symmetric) eigenvalue problem

$$\underline{\mathbf{K}}\mathbf{u} = \omega^2 \underline{\mathbf{M}}\mathbf{u} \quad (5.2)$$

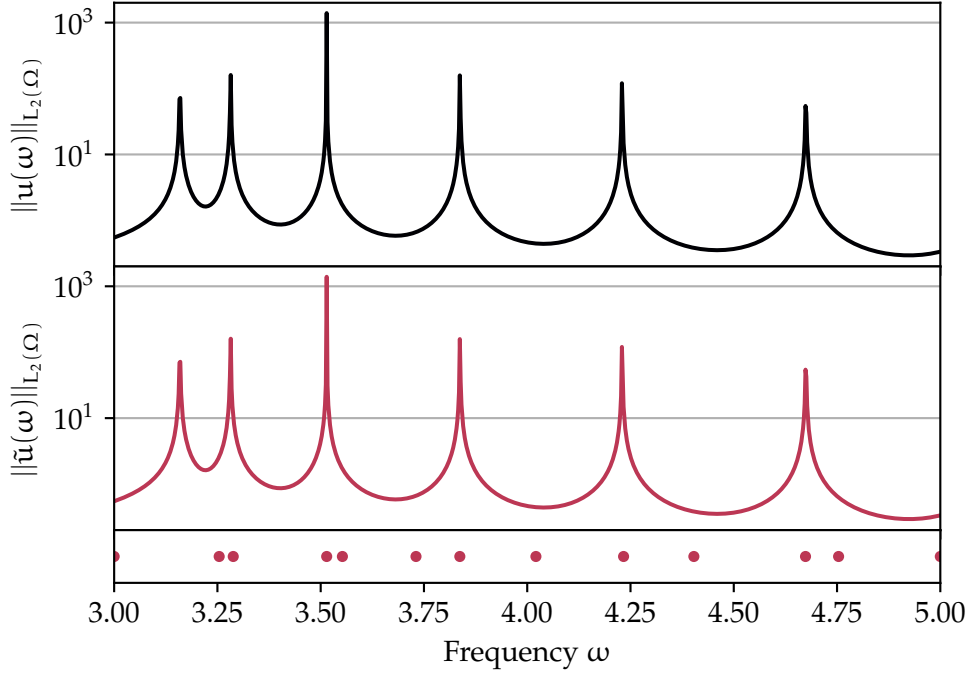


FIGURE 5.3 – Caption.

TABLE 5.1 – Comparison eigsh and gMRI.

	eigsh		gMRI	
DOF	Δ	t	Δ	t
713	1.950×10^{-2}	25.9 ± 1.1 ms	1.950×10^{-2}	61.9 ± 3.6 ms
7412	1.826×10^{-3}	199.0 ± 9.9 ms	1.827×10^{-3}	410 ± 16.8 ms
74722	1.817×10^{-4}	3.5 ± 0.1 s	1.820×10^{-4}	5.2 ± 0.2 s
745513	1.811×10^{-5}	75.0 ± 1.6 s	1.846×10^{-5}	104.0 ± 1.1 s

Take $\{\mathbf{u}_j, \omega_j^2\}_j$ be the resonant modes, i.e. solutions to the eigenvalue problem (5.2), such that

$$\underline{\mathbf{K}}\mathbf{u}_j = \omega_j^2 \underline{\mathbf{M}}\mathbf{u}_j \quad (5.3)$$

Adding a source term \mathbf{f}

$$\underline{\mathbf{K}}\mathbf{u} - \omega^2 \underline{\mathbf{M}}\mathbf{u} = \mathbf{f} \quad (5.4)$$

If \mathbf{u} is expressed in terms of the basis $\{\mathbf{u}_j\}_j$, i.e. $\mathbf{u} = \sum_j \alpha_j \mathbf{u}_j$

$$\sum_j \alpha_j (\underline{\mathbf{K}}\mathbf{u}_j - \omega^2 \underline{\mathbf{M}}\mathbf{u}_j) = \mathbf{f} \quad (5.5)$$

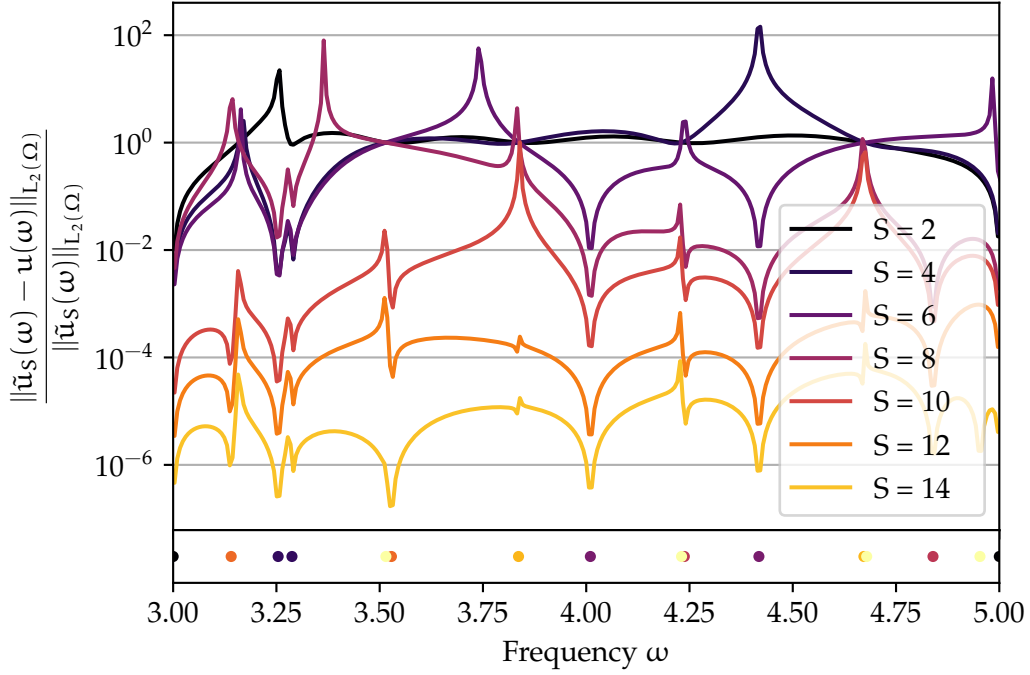


FIGURE 5.4 – Caption.

Using (5.3)

$$\sum_j \alpha_j (\omega_j^2 - \omega^2) \underline{\mathbf{M}} \mathbf{u}_j = \mathbf{f} \quad (5.6)$$

from which we can take the scalar product with \mathbf{u}_j^H to obtain

$$\alpha_j = \frac{\mathbf{u}_j^H \mathbf{f}}{\omega_j^2 - \omega^2} \quad (5.7)$$

If $\mathbf{u}_j^H \mathbf{f} = 0$, then the resonant mode at ω_j is suppressed (fine with MRI, but eigsh will detect a resonant mode).

For $\|\mathbf{u}\|_{L_2(\Gamma)}^2 = \int_{\Gamma} \|\mathbf{u}\|^2$

5.2 IMPERFECTLY CONDUCTING BOUNDARIES

Numerical eigenfrequencies, solve

$$(\underline{\mathbf{K}} - i\omega \underline{\mathbf{I}} - \omega^2 \underline{\mathbf{M}}) \mathbf{u} = 0 \quad (5.8)$$

Define $\mathbf{v} = \omega \mathbf{u}$, so that we may write this as the generalized eigenvalue problem

$$\begin{bmatrix} \underline{\mathbf{K}} & \underline{\mathbf{1}} \\ \underline{\mathbf{K}} & -i\underline{\mathbf{I}} \end{bmatrix} \begin{bmatrix} \mathbf{u} \\ \mathbf{v} \end{bmatrix} = \omega \begin{bmatrix} \underline{\mathbf{1}} & \\ & \underline{\mathbf{M}} \end{bmatrix} \begin{bmatrix} \mathbf{u} \\ \mathbf{v} \end{bmatrix} \quad (5.9)$$

which is, however, no longer Hermitian (LHS chosen as “diagonal” as possible).

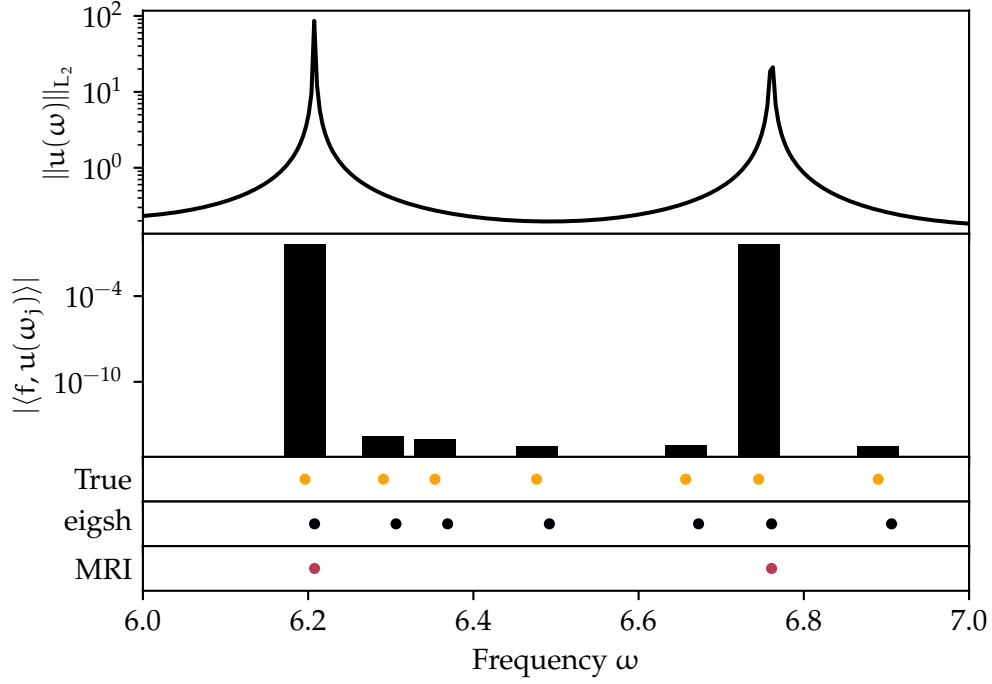


FIGURE 5.5 – Caption.

TABLE 5.2 – Comparison eigsh and gMRI.

	eigsh	gMRI
DOF	t	t
713	65.1 ± 2.48 ms	78.5 ± 7.4 ms
7412	906.0 ± 115.0 ms	496.0 ± 53.8 ms
74722	20.4 ± 0.3 s	6.2 ± 0.3 s

5.3 DUAL MODE CIRCULAR WAVEGUIDE FILTER

Modeled according to [5] in the computer-aided design modeler software application FreeCAD¹. Mesh generated using Gmsh². 5 smoothing steps, element size factor of 0.2 and Delaunay 3D meshing algorithm. The mesh was refined around critical components such as the screws and irises using transfinite curves. Conversion using meshio³ to .xml format which can be understood by FEniCS.

[1]

$$\underline{\mathbf{S}}(\omega) = \underline{\mathbf{1}} - 2 \left(\underline{\mathbf{1}} + i \frac{\omega}{2\pi} \sqrt{\frac{1 - (\omega_c/\omega_0)^2}{1 - (\omega_c/\omega)^2}} \underline{\mathbf{F}}^H \underline{\mathbf{U}}(\omega) \right)^{-1} \quad (5.10)$$

¹<https://www.freecadweb.org/>

²<https://gmsh.info/>

³<https://github.com/nschloe/meshio>

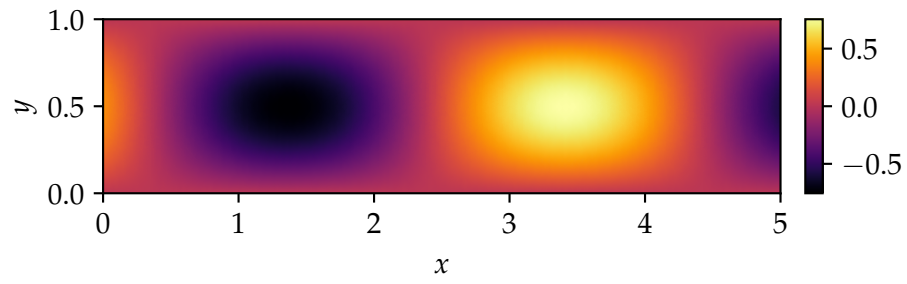


FIGURE 5.6 – $\omega = 3.5$.

with $\underline{\mathbf{F}} = [\mathbf{f}_1, \mathbf{f}_2]$ and $\underline{\mathbf{U}} = [\mathbf{u}_1, \mathbf{u}_2]$ with \mathbf{f}_1 the term resulting when forcing from one side producing the solution \mathbf{u}_1 , and the \mathbf{f}_2 when forcing from the other side to produce \mathbf{u}_2 .

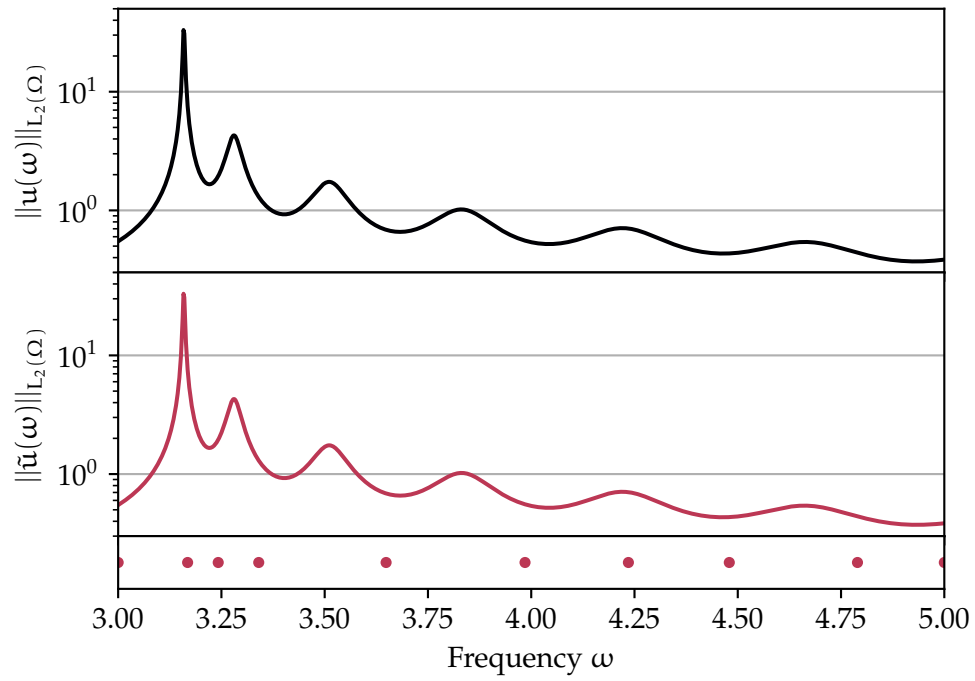


FIGURE 5.7 – Caption.

6 CONCLUSION AND OUTLOOK

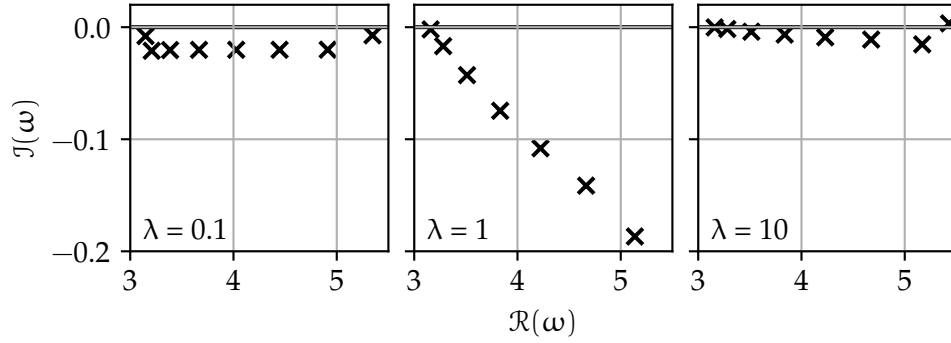


FIGURE 5.8 – Spurious resonant frequency far away from others and definitely not of interest for this problem, but indeed for rational surrogate.

REFERENCES

- [1] F. Nobile D. Pradovera. Frequency-domain non-intrusive greedy model order reduction based on minimal rational approximation. pages 159–167, 2021. doi: 10.1007/978-3-030-84238-3_16.
- [2] I. Perugia F. Bonizzoni, F. Nobile. Convergence analysis of padé approximations for helmholtz frequency response problems. *ESAIM: M2AN*, 52(4):1261 – 1284, 2018. doi: 10.1051/m2an/2017050.
- [3] M. Ruggeri F. Bonzzoni, D. Pradovera. Rational-based model order reduction of helmholtz frequency response problems with adaptive finite element snapshots. doi: 10.48550/arXiv.2112.04302.
- [4] A. Logg H. P. Langtangen. *Solving PDEs in Python: The FEniCS Tutorial I*. Springer, 2016. ISBN 978-3-319-52461-0. doi: 10.1007/978-3-319-52462-7.
- [5] J. Zapata J. R. Montejo-Garai. Full-wave design and realization of multicoupled dual-mode circular waveguide filters. *IEEE Transactions on Microwave Theory and Techniques*, 43(6):1290 – 1291, 1995.
- [6] F. Kagerer. Finite elements for maxwell’s equations, 2018.
- [7] G. Klein. Applications of linear barycentric rational interpolation, 2012.
- [8] P. Monk. *Finite Element Methods for Maxwell’s Equations*. Oxford Science Publications, 2003. ISBN 0-19-850888-3.
- [9] D. Pradovera. Model order reduction based on functional rational approximants for parametric pdes with meromorphic structure, 2021.
- [10] L. N. Trefethen. Householder triangularization of a quasimatrix. *IMA Journal of Numerical Analysis*, 30(4):887–897, 2010. doi: 10.1093/imanum/drp018.

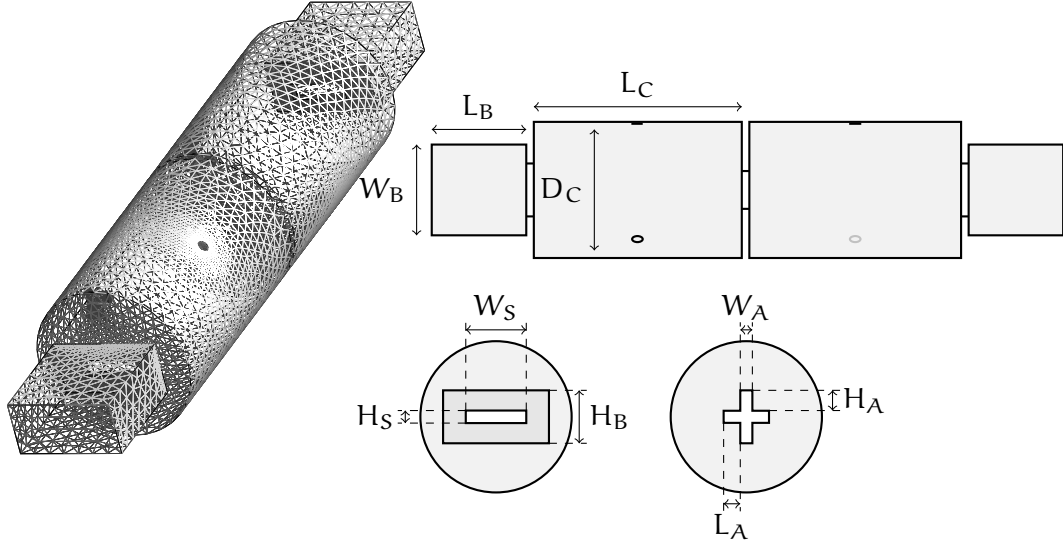


FIGURE 5.9 – Dual-mode circular waveguide filter. [5] $W_C = 43.87$ mm, $D_C = 28.0$ mm, $L_B = 43.87$ mm, $W_B = 19.05$ mm, $H_B = 9.525$ mm, $L_C = 20.0$ mm, $W_S = 10.05$ mm, $H_S = 3.0$ mm, $W_A = 2.0$ mm, $H_A = 3.375$ mm, $L_A = 2.825$ mm, thickness of all irises 2.0 mm, screws half way up the cavity horizontal tuning screws with depth 3.82 mm and coupling screws at angles $\pm 45^\circ$ with depth 3.57 mm.

7 APPENDIX

7.1 DETAILED DERIVATION FOR THE WEAK FORMULATION OF THE TIME-HARMONIC POTENTIAL EQUATION

The goal is to rewrite the curl-integral on the left-hand side of (2.12):

$$\int_{\Omega} (\nabla \times (\mu^{-1} \nabla \times \mathbf{u})) \cdot \mathbf{v} \quad (7.1)$$

In order to simplify the curls and apply the Gauss theorem, I first show the following vector calculus identity:

Curl product rule

$$(\nabla \times \mathbf{a}) \cdot \mathbf{b} = \nabla \cdot (\mathbf{a} \times \mathbf{b}) + \mathbf{a} \cdot (\nabla \times \mathbf{b}) \quad (7.2)$$

where \mathbf{a} , \mathbf{b} are vector-value functions. The completely antisymmetric tensor ε_{ijk} , frequently referred to as the Levi-Civita tensor, may be employed to rewrite the components of the curl of a vector-function \mathbf{a} as the sum

$$(\nabla \times \mathbf{a})_k = \sum_i \sum_j \varepsilon_{ijk} \partial_i u_j \quad (7.3)$$

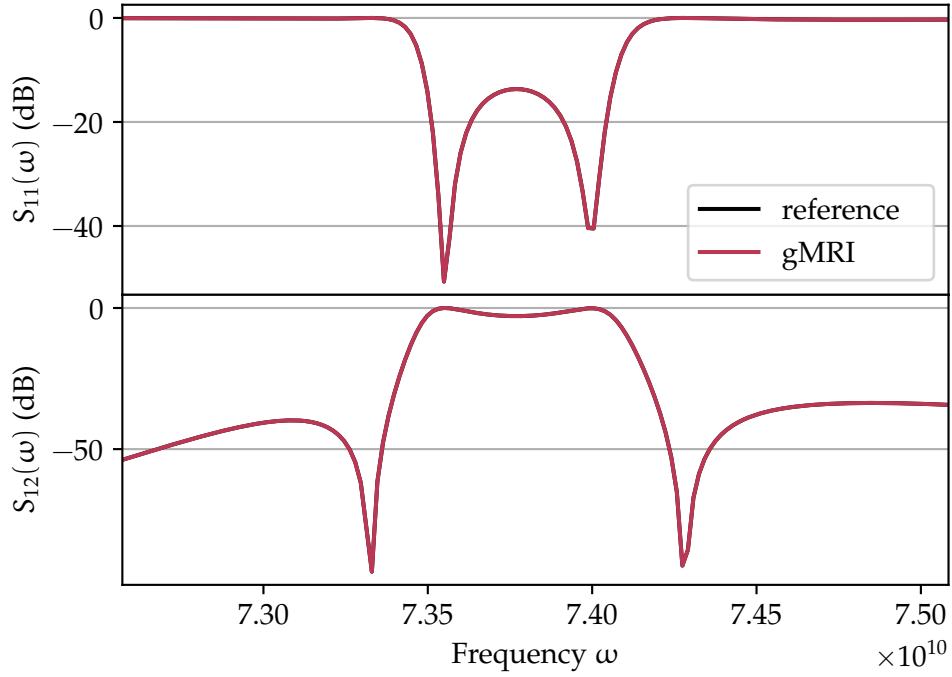


FIGURE 5.10 – Caption.

where ∂_i denotes the partial derivative with respect to the i -th coordinate direction. This yields

$$\begin{aligned}
 (\nabla \times \mathbf{a}) \cdot \mathbf{b} &= \sum_k (\nabla \times \mathbf{a})_k b_k \\
 &= \sum_k \left(\sum_i \sum_j \varepsilon_{ijk} \partial_i a_j \right) b_k \\
 &= \sum_k \sum_i \sum_j \partial_i (\varepsilon_{ijk} a_j b_k) - \sum_k \sum_i \sum_j a_j (\varepsilon_{ijk} \partial_i b_k) \\
 &= \sum_k \sum_i \sum_j \partial_i (\varepsilon_{jki} a_j b_k) - \sum_k \sum_i \sum_j a_j ((-\varepsilon_{ikj}) \partial_i b_k) \\
 &= \sum_i \partial_i (\mathbf{a} \times \mathbf{b})_i + \sum_j u_j (\nabla \times \mathbf{b})_j \\
 &= \nabla \cdot (\mathbf{a} \times \mathbf{b}) + \mathbf{a} \cdot (\nabla \times \mathbf{b})
 \end{aligned} \tag{7.4}$$

by expressing the scalar product as a component-sum, using the product rule and applying the symmetry and anti-symmetry properties of the Levi-Civita tensor. Now

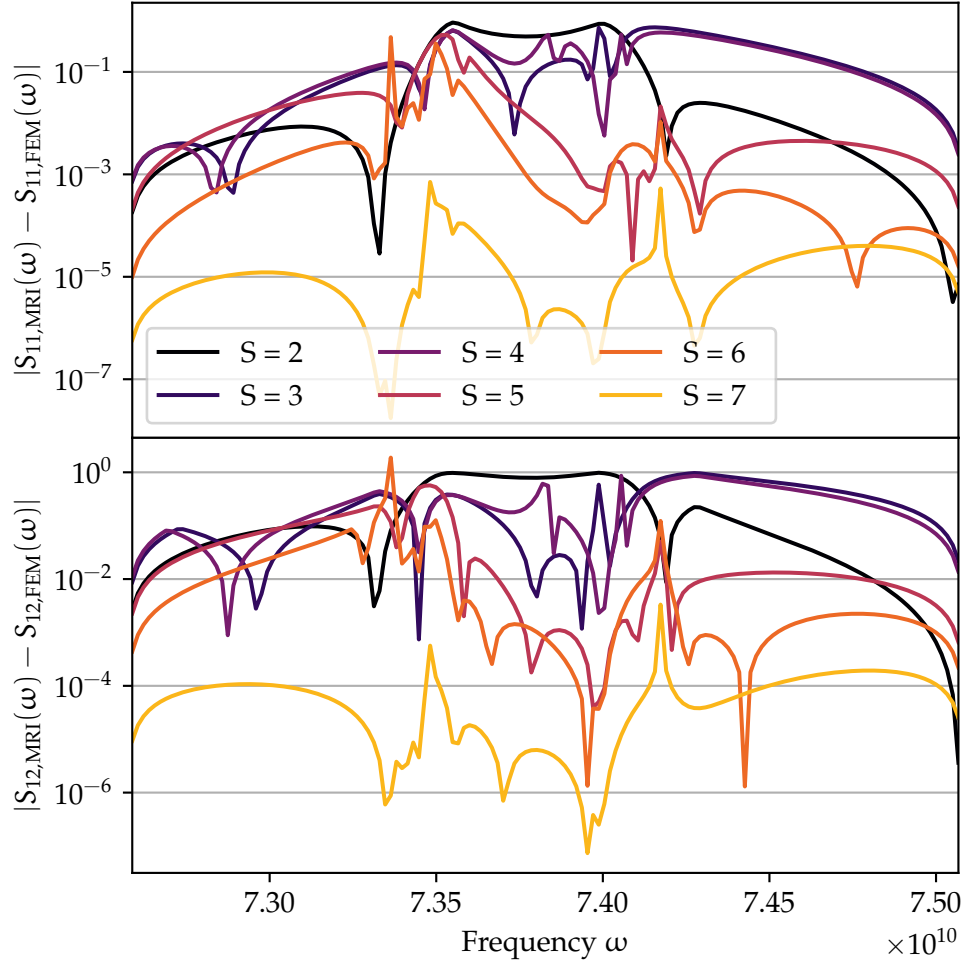


FIGURE 5.11 – Caption.

the identity (7.2) to (7.1) together with Gauss' theorem gives

$$\begin{aligned}
 \int_{\Omega} (\nabla \times (\mu^{-1} \nabla \times \mathbf{u})) \cdot \mathbf{v} &= \int_{\Omega} \nabla \cdot ((\mu^{-1} \nabla \times \mathbf{u}) \times \mathbf{v}) + \int_{\Omega} (\mu^{-1} \nabla \times \mathbf{u}) \cdot (\nabla \times \mathbf{v}) \\
 &= \int_{\partial\Omega} ((\mu^{-1} \nabla \times \mathbf{u}) \times \mathbf{v}) \cdot \mathbf{n} + \int_{\Omega} (\mu^{-1} \nabla \times \mathbf{u}) \cdot (\nabla \times \mathbf{v})
 \end{aligned}
 \tag{7.5}$$

For later convenience, the boundary integral can further be simplified using the

Commutative behavior of the scalar triple product

$$(\mathbf{a} \times \mathbf{b}) \cdot \mathbf{c} = -(\mathbf{a} \times \mathbf{c}) \cdot \mathbf{b}
 \tag{7.6}$$

This identity follows immediately from a small manipulation with the Levi-

Civita tensor:

$$\begin{aligned}
(\mathbf{a} \times \mathbf{b}) \cdot \mathbf{c} &= \sum_k \left(\sum_i \sum_j \varepsilon_{ijk} a_i b_j \right) c_k \\
&= \sum_j \left(\sum_i \sum_k (-\varepsilon_{ikj}) a_i c_k \right) b_j \\
&= -(\mathbf{a} \times \mathbf{c}) \cdot \mathbf{b}
\end{aligned} \tag{7.7}$$

The boundary integral becomes

$$\int_{\partial\Omega} ((\mu^{-1} \nabla \times \mathbf{u}) \times \mathbf{v}) \cdot \mathbf{n} = - \int_{\partial\Omega} ((\mu^{-1} \nabla \times \mathbf{u}) \times \mathbf{n}) \cdot \mathbf{v} \tag{7.8}$$

This concludes the short derivation, because now (7.1) may be rewritten as

$$- \int_{\partial\Omega} ((\mu^{-1} \nabla \times \mathbf{u}) \times \mathbf{v}) \cdot \mathbf{n} + \int_{\Omega} (\mu^{-1} \nabla \times \mathbf{u}) \cdot (\nabla \times \mathbf{v}) \tag{7.9}$$

I would also like to demonstrate that

Curl product rule

If $\mathbf{n} \perp \mathbf{u}$ and $\|\mathbf{n}\| = 1$, then

$$(\mathbf{n} \times \mathbf{u}) \times \mathbf{n} = \mathbf{u} \tag{7.10}$$

I again resort to the old faithful Levi-Civita tensor which satisfies the identity

$$\sum_i \varepsilon_{jki} \varepsilon_{lmi} = \delta_{jl} \delta_{km} - \delta_{jm} \delta_{kl} \tag{7.11}$$

Furthermore, I make use of the invariance of the tensor under cyclic permutation of the indices to obtain

$$\begin{aligned}
[(\mathbf{n} \times \mathbf{u}) \times \mathbf{n}]_k &= \sum_i \sum_j \varepsilon_{ijk} (\mathbf{n} \times \mathbf{u})_i n_j \\
&= \sum_i \sum_j \varepsilon_{ijk} \sum_l \sum_m \varepsilon_{lmi} n_l u_m n_j \\
&= \sum_i \sum_j \sum_l \sum_m \varepsilon_{jki} \varepsilon_{lmi} n_l u_m n_j \\
&= \sum_j \sum_l \sum_m (\delta_{jl} \delta_{km} - \delta_{jm} \delta_{kl}) n_l u_m n_j \\
&= \sum_j n_j u_k n_j - \sum_j n_k u_j n_j \\
&= \|\mathbf{n}\|^2 u_k - (\mathbf{u} \cdot \mathbf{n}) n_k \\
&= u_k
\end{aligned} \tag{7.12}$$

which concludes the component-wise proof.